

24 **Abstract**

25 We validate sea surface salinity (SSS) retrieved from Aquarius instrument on SAC-D
26 satellite with in situ measurements by Argo floats and moored buoy arrays. We assess the
27 error structure of three Aquarius SSS products: the standard product processed by
28 Aquarius Data Processing System (ADPS) and two datasets produced at the Jet
29 Propulsion Laboratory (JPL): the Combined Active-Passive algorithm with and without
30 rain correction, CAP and CAP_RC respectively. We examine the effect of various filters
31 to prevent unreliable point retrievals from entering Level-3 averaging, such as land or ice
32 contamination, radio-frequency-interference (RFI), and cold water.

33 Our analyses show that Aquarius SSS agrees well with Argo in a monthly average
34 sense between 40°S and 40°N except in the Eastern Pacific Fresh Pool and Amazon
35 River outflow. Buoy data within these regions show excellent agreement with Aquarius
36 but have discrepancy with the Argo gridded products. Possible reasons include strong
37 near surface stratification and sampling problems in Argo in regions with significant
38 western boundary currents. We observe large root-mean-square (RMS) difference and
39 systematic negative bias between ADPS and Argo in the tropical Indian Ocean and along
40 the Southern Pacific Convergence Zone. Excluding these regions removes the suspicious
41 seasonal peak in the monthly RMS difference between the Aquarius SSS products and
42 Argo. Between 40°S and 40°N, the RMS difference for CAP is less than 0.22 PSU for all
43 28 months, CAP_RC has essentially met the monthly 0.2 PSU accuracy requirement,
44 while that for ADPS fluctuates between 0.22 and 0.3 PSU.

45

46

47 **1. Introduction**

48 SSS is a critically important parameter relating the global water cycle to the
49 ocean circulation. As a joint venture by National Aeronautics and Space
50 Administration (NASA) and Comisión Nacional de Actividades Espaciales (CONAE),
51 the Aquarius/SAC-D (Satelite de Application Cientificas-D) was launched in June
52 2011 [*Lagerloef et al.* 1995, 2008; *Le Vine et al.* 2007]. Aquarius has been in
53 operation since 25 August 2011, providing unprecedented combined passive/active
54 L-band observations. The primary objective of Aquarius is to provide SSS maps to
55 monitor the seasonal and interannual variations of the large-scale features of SSS
56 with a spatial resolution of 150 km and retrieval accuracy of 0.2 PSU globally on a
57 monthly average basis. Performance statistics and analyses of residual errors are
58 documented in publications along the course of the Aquarius calibration/validation,
59 algorithm improvement, and release of various versions of data [e.g. *Lagerloef et al.*,
60 2013a; *Ebuchi and Abe*, 2012; *Ratheesh et al.* 2013]. In this study, we present results
61 of the error assessment for three Aquarius SSS products: the standard product
62 based on the algorithm developed at the Remote Sensing Systems (REMSS) and
63 operationally processed by the Aquarius Data Processing System (ADPS), and the
64 two datasets retrieved at JPL: CAP and CAP_RC. We used Aquarius V2.7.1 [pre-release
65 of V3.0] level-2 data for all three products.

66 We compare each of the Aquarius SSS products with in situ measurements using
67 Argo (Array for Real-time Geostrophic Oceanography) [*Roemmich and the Argo*
68 *Steering Team*, 2009] floats in the global oceans, and the salinity reports from the moored
69 buoys in the global tropics [*McPhaden*, 1995, *McPhaden et al.* 1998, *Bourles et al.*, 2008,

70 *Servain et al. 1998, McPhaden et al. 2009*]. With comparable accuracy of 0.01-0.02 PSU
71 [*Freitag et al., 1999; Hosoda et al., 2010*], Argo floats and moored buoys are
72 complimentary to each other in providing ground truth. Argo floats cover open oceans
73 with an average sampling rate of one observation every 10 days for each 3°x3° area.
74 Argo is the best available source with consistent global coverage that can be used to
75 assess Aquarius SSS performance, however it may not be sufficient to depict processes
76 with rapid temporal variability. Moreover, the shallowest depth where Argo floats can
77 operate reliably is 5-meters below the surface, where salinity may largely differ from that
78 from Aquarius in regions with high near surface stratification. On the other hand, the
79 moored buoys provide daily salinity measurements at 1-meter depth, which provide
80 measurements nearer to the surface and with higher temporal sampling. However, buoy
81 locations are sparse and the data records at each position may be discontinuous.

82 In Section 2 we describe the datasets of in situ measurements and Aquarius SSS
83 analyzed in this study. The comparisons of Aquarius products with Argo and buoy data
84 are presented in Section 3 and 4 respectively. In Section 5, we present error assessment of
85 the Aquarius SSS on monthly basis against Argo, but with certain areas excluded as
86 justified by buoy comparison. Finally a summary is given in Section 6.

87

88 **2. Data**

89 2.1. Argo floats

90 The Argo project provides in situ salinity profiles over the global ocean through the
91 deployment of over 3000 free-drifting profiling floats that measure salinity and
92 temperature from near the surface to 2000 dbar [*Roemmich and the ARGO team, 2009*].

93 This study uses both individual Argo float data and monthly gridded fields for evaluation.
94 We obtain the quality controlled individual Argo data collocated with Aquarius point
95 observations within 75 km and 4.5 days from the Aquarius Validation Data System
96 (AVDS) operated by Earth and Space Research (ESR). The spatial and temporal
97 collocation criteria were chosen to gather all ARGO floats within Aquarius footprint
98 (~100 km) in the 7-day orbit repeat cycle [*Lagerloef et al.*, 2013a].

99 Monthly gridded Argo data generated from float observations through optimal
100 interpolation (OI) are obtained from two sources. The first set is from the Asia-Pacific
101 Data-Research Center (APDRC) of the International Pacific Research Center (IPRC) at
102 the University of Hawaii (available from <http://apdrc.soest.hawaii.edu>). The second is
103 available from the Japan Agency for Marine-Earth Science and Technology (JAMSTEC)
104 (available from <http://www.jamstec.go.jp/ARGO>) [*Hosoda et al.*, 2010]. In contrast to the
105 APDRC, which is solely composed of Argo data, JAMSTEC combines data from ARGO
106 floats, Triangle Trans-Ocean Buoy Network (TRITON), and available conductivity-
107 temperature-depth (CTD) casts. In this study, we will focus on APDRC monthly gridded
108 ARGO data, for the convenience of identifying error sources. We will use the OI error
109 estimations, which are available in JAMSTEC dataset but not in APDRC, to confirm and
110 explain some regional discrepancies observed between Argo OI and Aquarius.

111

112 2.2. Moored buoys

113 Time series of daily salinity are collected at mooring stations from the global tropical
114 moored buoy array which includes the Tropical Atmosphere Ocean (TAO)/TRITON
115 array in the Pacific [*McPhaden*, 1995, *McPhaden et al.* 1998], the Pilot Research Moored

116 Array in the Tropical Atlantic (PIRATA) array [*Servain et al.*, 1998, *Bourles et al.*, 2008],
117 and the Research Moored Array for Africa-Asian-Australian Monsoon Analysis and
118 Prediction (RAMA) in the Indian Ocean [*McPhaden et al.*, 2009]. The TAO Project
119 Office of the National Oceanic and Atmospheric Administration (NOAA) and the Pacific
120 Marine Environmental Laboratory (PMEL) provide near-real-time daily-averaged surface
121 and subsurface data from moorings (available at www.pmel.noaa.gov/tao). The salinity
122 sensors maintained at each buoy provide internally recorded temperature and
123 conductivity data at 10-minute intervals, which are used to compute hourly averaged
124 salinity with accuracy of 0.02 PSU [*Freitag et al.*, 1999]. At most array sites, the vertical
125 profiles consists of measurements in the top 100 to 200 meters, but the depths at which
126 salinity measurements are available varies with location. In this study, we only consider
127 the highest and default quality control values, as provided in the data product.

128

129 2.3. Aquarius SSS

130 The standard Aquarius SSS product is based on the algorithm developed by REMSS
131 [*Meissner and Wentz*, 2014], operationally processed by ADPS and distributed by the
132 Physical Oceanography Distributed Active Archive Center (PODAAC). Also available
133 at PODAAC are the research datasets produced JPL, the CAP and CAP_RC products
134 [*Yueh and Chaubell*, 2012; *Yueh et al.*, 2013 and 2014]. The CAP algorithm retrieves the
135 salinity, wind speed, and direction simultaneously by minimizing the sum of the squared
136 differences between observations and model predictions. The CAP retrieval software can
137 be easily modified to account for additional geophysical quantities such as rain [*Tang et*
138 *al.*, 2013, 2014] and significant wave height [*Yueh et al.*, 2014]. SSS retrieval under rainy

139 conditions is challenging because the effects of surface freshening associated with rain
140 fresh water inputs and rain-induced surface roughness are mixed in the radiometric
141 signatures. Moreover, there are no extensive measurements of salinity in the upper few
142 centimeters that can be used to effectively separate these effects in radiometric signatures.
143 The current Geophysical Model Function (GMF) for ADPS and CAP were developed
144 using rain-free data. Applying the rain-free GMF to SSS retrieval under rainy conditions
145 is equivalent to attributing rain-induced signature completely to surface freshening and
146 ignoring its roughness effect, resulting in erroneously low salinity in the satellite retrieval.
147 Based on analyses of Aquarius L-band radar/radiometer signals under rainy conditions,
148 *Tang et al.* [2013] developed a rain correction scheme for GMF calibrated using salinity
149 from the HYbrid Coordinate Ocean Model (HYCOM) [*Chassignet et al.*, 2009] as a
150 reference. The uncertainty associated with using HYCOM SSS as reference for rain
151 correction model is discussed in *Tang et al.* [2014]. In this study, two sets of SSS are
152 retrieved in parallel with JPL CAP processing system, using GMF with and without rain
153 correction (referred as CAP_RC and CAP respectively). The ancillary surface rain rate
154 data used for rain correction is from Special Sensor Microwave Imager/Sounder
155 (SSM/I) F17 [*Wentz*, 1997; *Wentz and Spencer*, 1998] and the polarimetric microwave
156 radiometer WindSAT [*Gaiser et al.*, 2004], collocated within one hour in time and 12.5
157 km in distance from the center of Aquarius footprints. No rain correction is performed if
158 neither SSM/I or WindSAT met with collocation criteria, which excludes about 20% of
159 the Level 2 data blocks. CAP and CAP_RC are identical when the matchup rain rate is
160 zero or missing.
161

162 3. Comparison with ARGO

163 3.1 Level 2 data validation with individual ARGO floats

164 First we compare Aquarius level 2 SSS data products with individual Argo float data.
165 AVDS routinely matches up Argo data to the closest Aquarius level 2 measurements
166 within 75km and with time window of ± 4.5 days. In this study, all Aquarius data within
167 75 km from the Argo location are spatially averaged. Argo data are generally sampled at
168 a shallowest depth of 3-5 meters from surface. Fig.1 shows the scatter plot of collocated
169 data from Aug. 25, 2011 to Dec. 31, 2012 with the RMS difference and bias summarized
170 in Table 1. We observe that the performance varies with incidence angles, with beam-1
171 the worst and beam-3 the best for all three Aquarius SSS products.

172 We also note that ADPS has smaller RMS difference than CAP or CAP_RC, with the
173 RMS difference of all beams combined at 0.495, 0.563 and 0.558 PSU for ADPS, CAP
174 and CAP_RC, respectively. Statistical significance tests suggest the differences between
175 these RMS difference values are significant beyond the 99% significance level. Note that
176 the retrievals for CAP and CAP_RC are independent from sample to sample, while the
177 ADPS retrievals have used the monthly SSS climatology to constrain the retrievals and
178 are thus correlated.

179 The ADPS V3.0 algorithm divides the retrieval process into multiple steps to account
180 for surface roughness effects. First the horizontally polarized radiometer brightness
181 temperature (T_{BH}) is used along with the radar backscatter to retrieve the surface wind
182 speed. This step requires the use of a monthly SSS climatology (SSS_C) because T_{BH} is a
183 function of salinity; as a result the retrieved wind speed (W_C) is a function of SSS_C . The
184 next step of the retrieval process uses W_C to compute the roughness corrections to T_{BH}

185 and vertically polarized brightness temperature (T_{BV}). A least-squared optimization is
186 then used to retrieve the salinity from the roughness-corrected T_{BH} and T_{BV} . Because W_C
187 and the resulting brightness temperature correction terms are functions of SSS_C , the
188 ADPS SSS is also influenced by SSS_C . When the measurement noise is small enough, it
189 can be shown through perturbation methods that the ADPS SSS is approximately a
190 linearly weighted sum of the SSS_C and the noisy SSS estimate from the Aquarius data
191 itself. Because the SSS_C is constant, it does not contribute to the standard deviation of the
192 difference with the individual Argo observations within the same month. Also because all
193 the ADPS retrievals from the same month (even from a different year) will contain the
194 same SSS_C , the ADPS SSS retrievals within the same month are correlated.

195 The use of monthly climatology in the ADPS processing has effectively introduced a
196 smoothing factor to reduce the standard deviation and RMS difference of retrievals
197 within each month, and as a result the ADPS retrievals within a month are not
198 independent. Therefore the relative magnitude of RMS difference with individual floats
199 for each orbit pass does not indicate the relative accuracy of ADPS, CAP, and CAP_RC
200 because of the “effective smoothing” applied in the ADPS product. On the other hand,
201 since CAP or CAP_RC point-wise retrievals are independent, monthly averaging more
202 effectively reduces the RMS difference (Table 2).

203

204 3.2 Level 3 data validation with Argo maps

205 Monthly gridded SSS fields (Level 3) are created for each Aquarius product, i.e.
206 ADPS, CAP and CAP_RC, for comparison with monthly gridded Argo data. For each
207 grid point on $1^\circ \times 1^\circ$ grid over global oceans, all level 2 data blocks within 111 km radius

208 are spatially averaged using Gaussian weighting with half-power distance of 75 km, then
209 temporally averaged over the month. It is noted that Aquarius Project delivers two
210 versions of level 3 ADPS monthly SSS: smoothed and non-smoothed. We uses our own
211 gridded monthly version of ADPS instead of using level 3 data available from the project
212 to ensure the exact same filtering and gridding procedure are used for all three products.
213 The results presented in this study are comparable with the non-smoothed version of
214 ADPS level 3 data.

215 As illustrated in Fig. 2 for March 2013, all three of Aquarius SSS products, ADPS,
216 CAP and CAP_RC, depict large-scale features of the surface salinity field over global
217 oceans similar to the Argo gridded product. We see features such as the high salinities
218 found in the subtropics of north and south Atlantic; the low salinities found in the eastern
219 Pacific fresh pool, in the southern tropical Indian Ocean, and under the Inter-Tropical
220 Convergence Zone (ITCZ) and the Southern Pacific Convergence Zone (SPCZ). Data
221 gaps along the coastline in the Aquarius SSS products are due to excluding Level 2 data
222 blocks with land or ice fraction greater than 0.001, to avoid potentially contaminated
223 retrievals entering Level 3. The Argo map is masked out where there is no Aquarius data.
224 We note that Aquarius products reveal more detailed structures than Argo in some
225 regions, for example, the eastern equatorial Pacific fresh pool, and the Amazon River
226 outflow area. This demonstrates the sampling advantage of Aquarius in capturing and
227 resolving high resolution and high frequency SSS variations.

228 Figure 3 depicts the seasonal evolution of the difference between the Aquarius SSS
229 and Argo gridded products. In the tropical Pacific, the zonally orientated narrow bands of
230 negative values of satellite minus Argo (blue) appears in the eastern Pacific early in the

231 year, expands westward, and reaches its maximum extent in October. This is associated
232 with the surface freshening from rainfall captured by Aquarius while missed by Argo. We
233 note that the negative difference pattern of CAP_RC is slightly weaker than CAP,
234 suggesting that CAP_RC accounts part of observed surface emissivity as rain-induced
235 roughness while still able to reveal the surface freshening under rainy conditions [*Tang et*
236 *al.*, 2014]. In the tropical Atlantic, the most outstanding feature is the lower salinities
237 observed by satellite, emerging from the Amazon River outflow region and migrating
238 northward along the coast as far as 20°N late in the year. There is no observable
239 difference between CAP and CAP_RC in this region, as expected for a non-rain related
240 process. In the high latitudes (poleward of 40°), all Aquarius SSS products have a
241 positive bias throughout the year, although this bias is much more severe for ADPS than
242 CAP or CAP_RC in magnitude and affected area. This is not only caused by larger
243 satellite measurement error in the area due to loss of the salinity signal in emissivity in
244 cold water, but also because of the fewer number of available samples from Argo floats
245 in these regions. Finally, we observe systematic negative biases in ADPS over large
246 areas, particularly in the southern tropical Indian Ocean and along the SPCZ.

247 In Figure 4 we show a scatter-plot containing in total over 220,000 pairs of Aquarius
248 SSS and Argo for latitudes between 40°S and 40°N using the 12 monthly average maps
249 in 2012. For ADPS, CAP and CAP_RC, the overall biases with respect to Argo are -
250 0.068, -0.023 and 0.005 PSU; and RMS differences of 0.276, 0.225 and 0.217 PSU
251 respectively (all different beyond 99% significance level). The region in Figure 4 with the
252 highest density of points (red) for CAP and CAP_RC lie along the diagonal line, while
253 that for ADPS is off the diagonal line, consistent with the large region of negative bias

254 observed in Fig. 3. There are two groups of outliers centered on 32.5 and 35.5 PSU in
255 Argo data, where the Aquarius SSS is several PSU lower than Argo. While the
256 distribution for outliers centered on 32.5 PSU are similar between ADPS, CAP and
257 CAP_RC, the group centered on 35.5 PSU is much smaller for CAP & CAP_RC than
258 ADPS. These outliers are apparently associated with the negative difference patches
259 observed in the tropical oceans (Fig. 3), which may result from the combination of
260 satellite retrieval error and Argo float sampling, or may be due to near surface
261 stratification. In attempt to isolate these factors, we conduct a series of monthly data
262 gridding with different quality control schemes. Aquarius radiometer flags in V2.7.1
263 provide information on potential contamination from moon, galaxy reflection, RFI,
264 roughness correction convergence, and satellite operational conditions (for details see
265 Aquarius User Guide for Aquarius Dataset Version 3.0) [PO.DAAC, 2014]. Based on
266 these flags, we test various quality control schemes to filter out unreliable Level 2 data
267 blocks in producing Level 3 monthly maps. We identified a set of flags (so called “red”
268 flags) as listed in Table 2, which may be effective in enhancing the performance of Level
269 3 data. Fig. 4 corresponds to the gridded data produced with all “red” flags switched off,
270 therefore should serve as a baseline. We generated a series of gridded datasets with
271 individual flags switched on to gauge the effect of each one for eliminating outliers. Fig.
272 5 shows the scatter plot with “unacceptable ascending/descending difference” flag
273 switched on. It is found that although overall RMS differences reduced to 0.250, 0.212
274 and 0.204 for ADPS, CAP and CAP_RC, respectively, the two groups of outliers are still
275 there. Table 2 summarizes the bias and RMS difference with individual flags turned on,
276 comparing with all “red flags” on or off. It shows with certain quality control, the RMS

277 difference of all Aquarius Level 3 products decreases, while flag 17 (which eliminates
278 pixels where the difference between measured and predicted brightness temperature
279 greater than 0.4 K) and flag 23 (which eliminates pixels with unacceptable
280 ascending/descending differences) seem to be most effective in reducing overall RMS
281 difference.

282 The RMS differences between Aquarius SSS and Argo gridded data from 40°S to
283 40°N are calculated for each month (Fig. 6). From September 2011 to December 2013,
284 the RMS differences for CAP and CAP_RC vary between 0.19 and 0.29 PSU, and for
285 ADPS between 0.24 and 0.32 PSU. The RMS differences for all three products seems to
286 have a seasonal cycle peaking in August-October, suggesting the existence of some
287 seasonal processes either affecting the performance of Aquarius retrieval algorithm or
288 interfering with the validation. Fig. 7 shows the resulting RMS differences of the monthly
289 data gridded with the “unacceptable ascending/descending differences” switched on. It
290 reduces the monthly RMS difference range to 0.18-0.26 for CAP and CAP_RC, and 0.22-
291 0.28 for ADPS, but the suspicious seasonal peaks remain.

292

293 **4. Comparison with moored buoys**

294 We downloaded the time series of daily salinity measured at 1-m depth by
295 TAO/PIRATA/RAMA moored buoys from www.pmel.noaa.gov/tao, from Sept.1, 2011
296 to Dec. 31, 2013. The Aquarius SSS daily records are created using all available Level 2
297 data blocks within 111 km from the buoy location and averaged using Gaussian
298 weighting with half-power distance of 75 km (similar to the Level 3 gridding in Section
299 3), only if there are more than 20 data blocks collocated. The Aquarius local sampling

300 interval varies by location, with at least one daily sample every 7 days in the tropics. To
301 be consistent with Level 3 monthly data validation (Sec. 3.2), a 30-day moving average is
302 applied to the time series of each product at each buoy location. The time series of Argo
303 at each buoy location is created in the same way from Argo matchups with Aquarius
304 level 2 data blocks obtained using spatial and temporal interpolation from Argo monthly
305 gridded data.

306 For example, Fig. 8 illustrates the time series at two representative locations from the
307 TAO [McPhaden, 1995, *McPhaden et al.* 1998] and RAMA [McPhaden et al, 2009]
308 arrays, respectively. In the western Pacific warm pool at 156°E on the Equator (Fig.8a),
309 the Aquarius SSS agrees very well with buoy 1-meter salinities over a period of more
310 than two years, including the annual/interannual variation over two seasonal cycles, as
311 well as the abrupt salinity changes over short periods. The biases are -0.22, -0.06 and
312 0.03 PSU for ADPS, CAP and CAP_RC respectively, with RMS differences of 0.25, 0.14
313 and 0.15. It is noted that in this region with frequent precipitation, the rain correction
314 eliminates the negative bias but may over correct for the rain-induced roughness resulting
315 in positive bias and RMS difference slightly larger than CAP. Comparison with buoys
316 also confirm that ADPS has systematic negative biases, consistent with previous
317 observations in comparison with Argo. In addition, the problem seems to become more
318 severe in the southern tropical Indian Ocean as shown in the time series at the RAMA
319 buoy located at 5°S, 95°E (Fig. 8b). Similar time series analyses are conducted on each
320 buoy location over the entire tropical moored buoy arrays, with results summarized in
321 Figs. 9 to 11.

322 Figure 9 shows color-coded correlation coefficients between buoy 1-m salinity and
323 each of the Aquarius SSS products at buoy locations. Note the number of available
324 samples varies from site to site due to non-uniform buoy operation across the array. We
325 only include buoys with more than 50 collocated daily samples available during the
326 period in this figure. The correlation between Aquarius and buoy is more than 0.8 at the
327 majority of locations, with a few exceptions e.g. the Bay of Bengal (15°N, 90°E), and in
328 the southeastern Pacific (8°S, 110°W). Although we attempt to use the buoy data with
329 only the highest quality, some buoy measurements seem suspicious. For instance, an
330 exceptionally large discrepancies between Aquarius SSS and buoy is observed at 8°S,
331 110°W, where the buoy showed a salinity drop of nearly 2 PSU from September 2011 to
332 May 2012, never recovered and ceased operations February 2013. In the meantime,
333 Aquarius depicted two seasonal cycles, and agreed well with Argo. Further investigation
334 is needed to understand whether these large discrepancies are caused by regional
335 processes (e.g. river runoff, ocean current) or buoy sensor failure. Overall, Fig. 9
336 indicates all three Aquarius SSS products are able to capture the temporal variability at
337 monthly or shorter time scales.

338 In contrast to the temporal correlation, the biases between Aquarius SSS and buoy
339 differ from each other between ADPS, CAP and CAP_RC (Fig. 10). Consistent with the
340 Argo comparison, ADPS shows negative biases as compared to buoy 1-m salinity almost
341 across the entire array.

342 The RMS differences between buoys and the Aquarius SSS over the entire tropical
343 moored buoy array are summarized in Fig. 11. The lowest RMS difference (about 0.1
344 PSU) is found in the central equatorial Pacific. We observe that CAP retrievals with rain

345 correction (CAP_RC) reduce the RMS difference in some areas, such as the western
346 tropical Pacific and northern Atlantic Ocean. For all three Aquarius products, the RMS
347 differences are particularly high in the Bay of Bengal, the southeastern Indian Ocean, and
348 in several scattered locations in the Pacific. Further investigations are needed to find out
349 the reasons behind these large RMS differences, which may vary from site to site. For
350 example, in the Bay of Bengal, this may be due to the fact that these locations are under
351 great influence of river runoff, where large sampling errors are expected due to imprints
352 of small-scale variability on the satellite footprints [Vinogradova and Ponte, 2013]; while
353 at location 8°S, 110°W in the the Pacific, this may caused by un-filtered bad
354 measurements from the buoy before its termination, as discussed earlier in this section.

355 Fig. 12 illustrates the distribution of the total 107 buoys for ADPS, CAP and
356 CAP_RC in terms of their respective bias and RMS difference with respect to the 1-m
357 buoy salinity. At nearly half of locations over the buoy array, CAP_RC has a bias less
358 than 0.05 PSU (centered at bias bin 0.0), while the distribution for ADPS peaks at -0.2
359 PSU, consistent with comparisons with Argo as described in Sec. 3. CAP and CAP_RC
360 also show a higher population at low RMS differences (< 0.15 PSU) than ADPS.

361

362 **5. Error Assessment**

363 We assess the retrieval error of the Aquarius SSS by combining evaluations with
364 Argo and buoy measurements. Fig. 13 shows the RMS difference with respect to Argo
365 calculated from 28 months of gridded data for ADPS, CAP and CAP_RC, respectively,
366 where the locations of the moored buoy arrays are overlaid. We are particularly
367 interested in two areas between 40°S and 40°N where a large discrepancy between all

368 three Aquarius SSS products and Argo is observed, such as in the Atlantic Ocean near the
369 Amazon River outflow, and in the Eastern Pacific Fresh Pool north of the Equator. At
370 two of these buoy locations (the white dots in Fig. 13) within those two regions, we show
371 a 30-days moving average of the Aquarius SSS, buoy 1-meter salinity, and Argo, as
372 shown in Fig. 14.

373 In the Eastern Pacific Fresh Pool, the TAO buoy at 2°N, 95°W (Fig.14a) provided
374 measurements from Sept. 2011 to March 2012 and March to Aug. 2013. During these
375 periods, buoy observations agreed better with Aquarius SSS than with Argo, with RMS
376 differences of 0.30, 0.22, 0.22 PSU for ADPS, CAP, CAP_RC, respectively, and 0.41
377 PSU for Argo. It appears Argo gridded products failed to capture the magnitude of the
378 two freshening events in February 2012 and May 2013. Unfortunately there are no buoy
379 measurements available to validate the freshening peak observed by Aquarius in
380 February 2013. Alory et al. (2012), using ship and the Soil Moisture and Ocean Salinity
381 (SMOS) data, depicted the quasi-permanent presence of eastern Pacific fresh pool with
382 SSS lower than 33 PSU and extending westward to 95°W in April. The vertical structure
383 of this fresh pool along 95°W can be seen in *McPhaden et al.* [2008]. We check the
384 monthly maps of Argo OI error estimation given in JAMSTEC dataset and confirm that
385 in this region Argo errors are consistently small (less than 0.05 PSU) (Fig. S1). We
386 believe that the strong near surface stratification associated with the freshening events
387 caused the large discrepancy between surface (observed by Aquarius) and 5-meters
388 below (observed by Argo).

389 On the other hand, the area of large RMS difference in the western tropical Atlantic
390 coincides with the area where Argo floats perform worst; as confirmed by the large Argo

391 OI error estimation (larger than 0.5 PSU) throughout the year (Fig. S1). This area is
392 influenced by the Amazon River outflow as Aquarius observed the low surface salinity
393 with detailed spatial features within a few weeks of mission start [Lagerloef et al., 2013].
394 Grodsky et al. (2012) have published a study of this region using Aquarius data on the
395 interaction of Hurricane Katia and the Amazon River outflow. Near the eastern edge of
396 this area, the PIRATA buoy [Servain et al., 1998, Bourles et al., 2008] at 8°N, 38°W
397 measurements are available from Sept. 2011 to Sept. 2012, and June to Sept. 2013, giving
398 RMSD of 0.23, 0.25, 0.25, and 0.55 for ADPS, CAP, CAP_RC and Argo, respectively.
399 Available buoy measurements cover important periods of the two early freshening stages
400 from June to Sept. in 2012, 2013, respectively, as well as the seasonal minimum salinity
401 in Oct. 2011 and its recovery afterwards. During these periods, buoy data agree very well
402 with Aquarius but shows large discrepancies with Argo (Fig.14b). It confirms that the
403 large RMS difference is caused by error in the monthly Argo data rather than Aquarius
404 SSS in this area, which is under the influence of strong western boundary currents
405 resulting in relatively low sampling rate by Argo floats [Roemmich and the Argo Steering
406 Team, 2009].

407 Based on the above analysis, we conclude Argo data is not appropriate to be used as
408 ground truth for validation in the areas where its temporal aliasing or operational depth
409 may result in unrealistic error assessments for Aquarius. Examples of these regions
410 include the area near the eastern Pacific fresh pool where near surface stratification are
411 strong [Alory et al., 2012, McPhaden et al., 2008]; and the area along the coast near
412 Amazon River outflow where Argo OI error is large [Fig. S1]. Fig. 15 shows the monthly
413 time series of RMS differences with respect to Argo calculated by excluding the two

414 patches of data indicated in Fig. 13. Compared with Fig. 6, which includes all grid points
415 between 40°S and 40°N, the monthly RMS difference with respect to Argo is greatly
416 improved, particularly the elimination of seasonal peaks in boreal summer. It appears that
417 CAP and CAP_RC gain more improvement than ADPS, with RMS difference for
418 CAP_RC below 0.2 PSU across the board except three months of Nov. 2011, March and
419 April of 2013. Statistics over the entire 28 months of gridded data are summarized in
420 Table 3.

421 We perform the Student's T-test on the samples of 28 months of RMS difference with
422 respect to Argo (Fig. 6, 7 & 15), on pairs of the Aquarius data products. Our results
423 indicate the RMS difference of ADPS is significantly different from that of either CAP or
424 CAP_RC at significance level above 99% in all cases. The significant different level
425 between CAP and CAP_RC is lower (~70%), which is not surprising due to the fact that
426 the effect of rain correction must be reduced with global averaging. In areas where
427 evaporation-minus-precipitation is the dominant driving force for the water cycle, e.g. in
428 ITCZ, *Tang et al.* [2014] found the difference between CAP and CAP_RC could cause
429 more than 10% difference in the intensity of upper ocean salinity storage tendency.

430

431 **6. Summary**

432 Three Aquarius SSS data products, ADPS, CAP and CAP_RC are validated with in-
433 situ measurements from Argo floats and moored buoys. Comparison of level 2 data with
434 individual Argo floats indicates ADPS has smaller RMS difference than CAP and
435 CAP_RC, likely due to the smoothing effect of monthly climatology constraints applied
436 in ADPS retrieval. As CAP and CAP_RC point-wise retrievals are independent, monthly

437 averaging results in greater noise reduction than ADPS, as compared to Argo or moorings.
438 Comparison of level 3 data with Argo monthly data shows Aquarius SSS depict the
439 global features and seasonal evolution in tropical oceans, but with large discrepancies
440 observed in high latitudes, areas near Amazon River outflow, in the ITCZ such as
441 particularly in Eastern Pacific Fresh Pool, and SPCZ. The RMS difference obtained
442 between 40°S and 40°N on monthly basis shows a suspicious seasonal peak in August.
443 Various filtering methods are tested using radiometer flags included in ADPS level 2 files
444 to prevent unreliable retrievals entering monthly average, which results in smaller RMS
445 difference, but the seasonal variation remains. In addition, we observed systematic
446 negative biases in the ADPS product over large areas in southern tropical Indian Ocean
447 and along SPCZ.

448 Comparison with daily 1-meter salinity measurements from moored buoy arrays
449 shows Aquarius SSS correctly depicts temporal variation at time scales shorter than
450 monthly. Statistics over entire buoy arrays suggests that CAP_RC performs the best in
451 terms of its un-skewed biases and higher population at low RMS difference, while it
452 confirms systematic negative biases observed in the ADPS products.

453 Using in situ buoy measurements, we identify areas where the Argo monthly data are
454 not appropriate to be used for Aquarius SSS validation. By excluding the two patches in
455 the Eastern Pacific Fresh Pool and near the Amazon River outflow, the monthly RMS
456 difference with respect to Argo between 40°S and 40°N is improved for all Aquarius SSS
457 data products, reduced to below 0.22 PSU for CAP for all 28 months, and below 0.2 PSU
458 for CAP_RC except three months. We emphasize that excluding those areas in validation
459 is done because the monthly Argo gridded products cannot serve as ground truth for

460 surface salinity due to its limited sampling and operational depth, while Aquarius SSS
461 should be useful for studies in those areas, as supported by available buoy measurements.

462

463 **Acknowledgement**

464 The work described in this paper was carried out by the Jet Propulsion Laboratory,
465 California Institute of Technology under a contract with the National Aeronautics and
466 Space Administration. Aquarius SSS data are available from <http://podaac.jpl.nasa.gov>;
467 Argo monthly gridded data from <http://apdrc.soest.hawaii.edu>; Argo individual floats
468 data collocated with Aquarius from <https://aquarius.esr.org/avds>; moored buoy data from
469 www.pmel.noaa.gov/tao.

470

471 **Reference**

472 Alory, G., C. Maes, T. Delcroix, N. Reul, and S. Illig (2012), Seasonal dynamics of sea
473 surface salinity off Panama: The far Eastern Pacific Fresh Pool, *J. Geophys. Res.*, 117,
474 C04028, doi:10.1029/2011JC007802.

475 Bourlès, B., R. Lumpkin, M.J. McPhaden, F. Hernandez, P. Nobre, E. Campos, L. Yu, S.
476 Planton, A. Busalacchi, A.D. Moura, J. Servain, and J. Trotte (2008), The PIRATA
477 Program: History, Accomplishments, and Future Directions. *Bull. Amer. Meteor. Soc.*,
478 89, 1111-1125.

479 Chassignet, E. P., H. E. Hurlburt, E. J. Metzger, O. M. Smedstad, J. Cummings, G. R.
480 Halliwell, R. Bleck, R. Baraille, A. J. Wallcraft, C. Lozano, H. L. Tolman, A.
481 Srinivasan, A. Hankin, P. Cornillon, R. Weisberg, A. Barth, R. He, F. Werner, and J.

482 Wilkin (2009), U.S. GODAE: Global Ocean Prediction with the HYbrid Coordinate
483 Ocean Model (HYCOM), *Oceanography*, 22(2), 64-75.

484 Ebuchi, N., and H. Abe (2012), Evaluation of sea surface salinity observed by Aquarius.
485 *Proc. IEEE Int. Geoscience and Remote Sensing Symp.*, Munich, Germany, IEEE,
486 Paper 2246.

487 Freitag, H.P., M.E. McCarty, C. Nosse, R. Lukas, M.J. McPhaden, and M.F. Cronin
488 (1999), COARE Seacat data: Calibrations and quality control procedures. *NOAA Tech.*
489 *Memo. ERL PMEL-115*, 89 pp.

490 Gaiser, P.W., K. M. St. Germain, E. M. Twarog, G. A. Poe, W. Purdy, D. Richardson, W.
491 Grossman, W. L. Jones, D. Spencer, G., Golba, J. Cleveland, L. Choy, R. M.
492 Bevilacqua, and P. S. Chang (2004), The Windsat Spaceborne Polarimetric
493 Microwave Radiometer: Sensor Description and Early Orbit Description, *IEEE Trans.*
494 *Geosci Remote Sens.*, 42(11), 2347-2361.

495 Grodsky, S. A., N. Reul, G. Lagerloef, G. Reverdin, J. A. Carton, B. Chapron, Y. Quilfen,
496 V. N. Kudryavtsev, and H.-Y. Kao (2012), Haline hurricane wake in the
497 Amazon/Orinoco plume: AQUARIUS/SACD and SMOS observation, *Geophys. Res.*
498 *Lett.*, 39, L20603, doi:[10.1029/2012GL053335](https://doi.org/10.1029/2012GL053335).

499 Hosoda, S., T. Ohira, K. Sato, and T. Suga (2010), Improved description of global mixed-
500 layer depth using Argo profiling floats, *J. Oceanogr.*, 66, 773-787.

501 Lagerloef, G., C. T. Swift, and D. M. Le Vine (1995), Sea surface salinity: The next
502 remote sensing challenge. *J. Oceanogr.*, 8, 44-50.

503 Lagerloef, G., Colomb Fr, Le Vine D, et al. (2008), The Aquarius/Sac-D Mission:
504 Designed To Meet The Salinity Remote-Sensing Challenge, *Oceanography*, Vol. 21,
505 Pages: 68-81.

506 Lagerloef, G. et al. (2013a). Aquarius Data Release V2.0 Validation Analysis. Aquarius
507 Project Document: AQ-014-PS-0016.

508 Lagerloef, G., A. deCharon, and E. Lindstrom (2013b), Ocean Salinity and the
509 Aquarius/SAC-D Mission: A New Frontier in Ocean Remote Sensing, *Marine*
510 *Technology Society J.*, Vol. 47, Pages: 26-30.

511 Le Vine, D. M., G. S.E. Lagerloef, F.R.Colomb, S.H. Yeh, and F.A. Pellerano (2007),
512 Aquarius: An instrument to monitor sea surface salinity from space. *IEEE Trans.*
513 *Geosci. Remote Sens.*, 45, 2040–2050.

514 McPhaden, M. J. (1995), The TAO array is completed. *Bull. Amer. Meteor. Soc.*, 76,
515 739–741.

516 McPhaden, M.J., A.J. Busalacchi, R. Cheney, J.R. Donguy, K.S. Gage, D. Halpern, M. Ji,
517 P. Julian, G. Meyers, G.T. Mitchum, P.P. Niiler, J. Picaut, R.W. Reynolds, N. Smith,
518 K. Takeuchi (1998), The Tropical Ocean-Global Atmosphere (TOGA) observing
519 system: A decade of progress. *J. Geophys. Res.*, 103, 14,169-14,240.

520 McPhaden, M.J., M.F. Cronin, and D.C. McClurg (2008), Meridional structure of the
521 surface mixed layer temperature balance on seasonal time scales in the eastern
522 tropical Pacific. *J. Climate*, 21, 3240-3260.

523 ———, and Coauthors (2009), RAMA: The Research Moored Array for African–Asian–
524 Australian Monsoon Analysis and Prediction. *Bull. Amer. Meteor. Soc.*, 90, 459–480.

525 Meissner, T. and F. Wentz (2014), A Geophysical model for the emission and scattering

526 of L-band microwave radiation from rough ocean surfaces, submitted to JGR.

527 Physical Oceanography Distributed Active Archive Center (PO.DAAC) (2014), Aquarius
528 User Guide, Aquarius Dataset Version 3.0, JPL D-70012, AQ-010-UG-0008.

529 Ratheesh, S., B. Mankad, S. Basu, R. Kumar, and R. Sharma (2013), Assessment of
530 Satellite-Derived Sea Surface Salinity in the Indian Ocean, *IEEE Trans. Geoscience
531 and Remote Sensing*, 10(3), 428-431.

532 Roemmich, D., and the Argo Steering Team (2009), Argo: The challenge of continuing
533 years of progress, *Oceanography*, 22, 46–55.

534 Servain, J., A. Busalacchi, M. McPhaden, A. Moura, G. Reverdin, M. Vienna, and S.
535 Zebiak (1998), A Pilot Research Moored Array in the Tropical Atlantic (PIRATA).
536 *Bull. Amer. Meteor. Soc.*, 79, 2019–2031.

537 Tang, W., S. H. Yueh, A. Fore, G. Neumann, A. Hayashi, and G. Lagerloef (2013), The
538 rain effect on Aquarius' L-band sea surface brightness temperature and radar
539 backscatter, *Remote Sensing of Environment*, 137, 147-157.

540 Tang, W., S. H. Yueh, A. Fore, A. Hayashi, T. Lee, and G. Lagerloef (2014), Uncertainty
541 of Aquarius sea surface salinity retrieved under rainy conditions and its implication
542 on the water cycle study. Submitted to JGR.

543 Vinogradova, N. T., and R. M. Ponte (2013), Small-scale variability in sea surface
544 salinity and implications for satellite-derived measurements. *J. Atmos. Oceanic
545 Technol.*, 30, 2689–2694. DOI: 10.1175/JTECH-D-13-00110.1.

546 Wentz, F. J. (1997), A well-calibrated ocean algorithm for SSM/I, *J. Geophys. Res.*, 102,
547 C4, 8703-8718.

548 Wentz, F. J., and R. W. Spencer (1998), SSM/I rain retrievals within a unified all-weather

549 ocean algorithm, *J. Atmos. Sci.*, 55, 1613–1627.

550 Yueh, S. H. and M. J. Chaubell (2012), Sea Surface Salinity and Wind Retrieval Using
551 Combined Passive and Active L-Band Microwave Observations, *IEEE Trans.*
552 *Geoscience and Remote Sensing*, 50(4), 1022-1032.

553 Yueh, S. H., W. Tang, A. Fore, G. Neumann, A. Hayashi, A. Freedman, J. Chaubell, and
554 G. Lagerloef (2013), L-band Passive and Active Microwave Geophysical Model
555 Functions of Ocean Surface Winds and Applications to Aquarius Retrieval. *IEEE*
556 *Trans. Geoscience and Remote Sensing*, 51(9), 4619-4632, DOI:
557 10.1109/TGRS.2013.2266915.

558 Yueh, S., W. Tang, A. Fore, A. Hayashi and Y. T. Song (2014), Aquarius Geophysical
559 Model Function and Combined Active Passive Algorithm for Ocean Surface Salinity
560 and Wind Retrieval, submitted to JGR.

561 Table 1. Bias and RMSD of Aquarius retrieved SSS (level 2) with respect to
 562 individual Argo floats matchups from August 25, 2011 to December 31, 2012.

(PSU)	Bias (Aquarius SSS – Argo)			RMSD		
	ADPS	CAP	CAP RC	ADPS	CAP	CAP RC
All beam	-0.020	0.041	0.074	0.495	0.563	0.558
Beam-1	-0.014	0.007	0.041	0.545	0.619	0.613
Beam-2	-0.022	0.073	0.107	0.487	0.547	0.546
Beam-3	-0.023	0.042	0.074	0.454	0.523	0.512

563 Table 2. Bias and RMS difference of monthly gridded data between 40°N and 40°S from
 564 Jan. – Dec., 2012.
 565

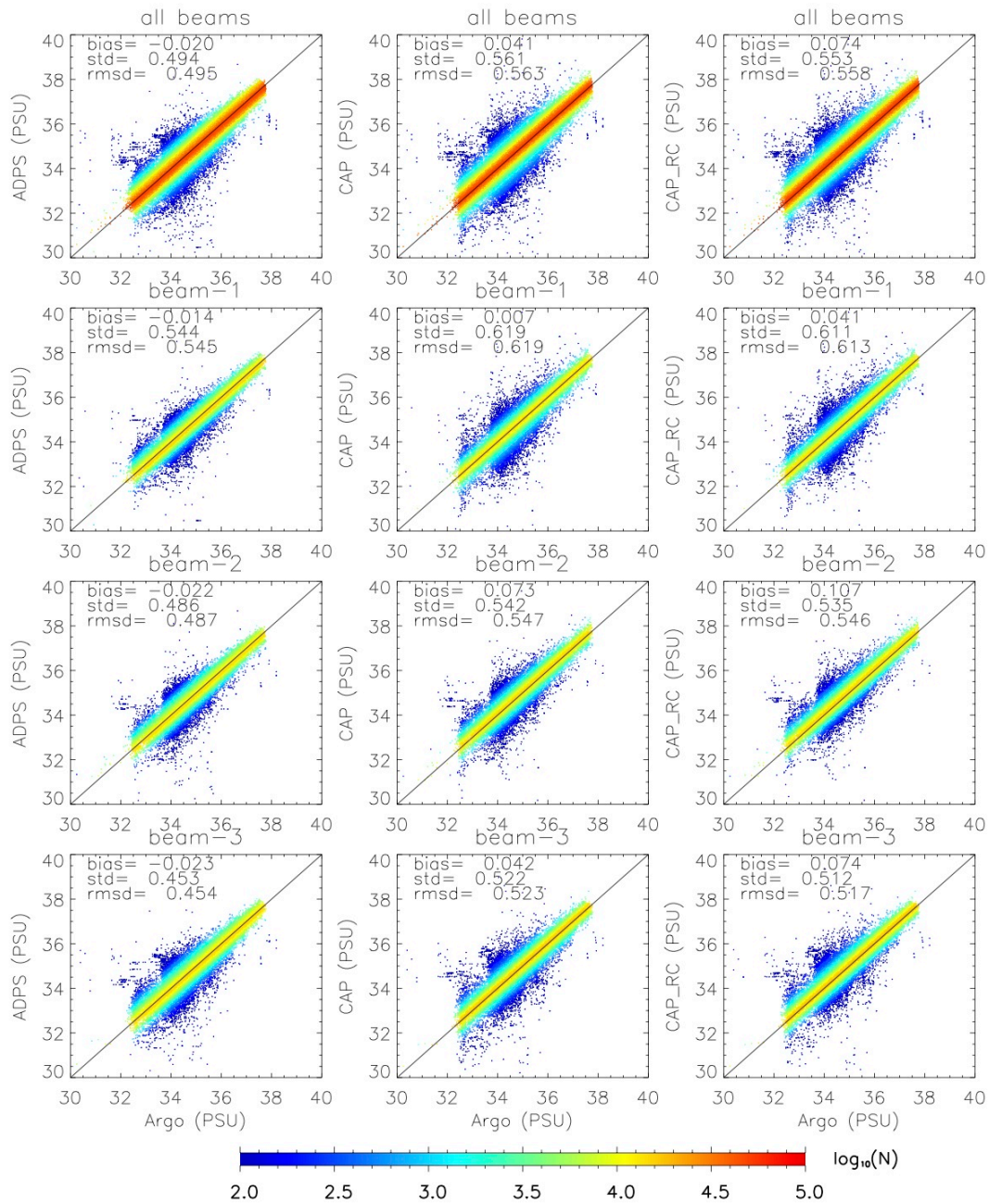
(PSU)	Bias (Aquarius SSS – Argo)			RMSD		
	ADPS	CAP	CAP RC	ADPS	CAP	CAP RC
All off	-0.068	-0.023	0.005	0.276	0.225	0.217
Flag5 on	-0.067	-0.021	0.008	0.276	0.226	0.218
Flag14 on	-0.066	-0.023	0.006	0.275	0.225	0.217
Flag17 on	-0.059	-0.021	0.007	0.245	0.215	0.207
Flag18 on	-0.068	-0.023	0.005	0.276	0.225	0.217
Flag19 on	-0.066	-0.021	0.007	0.272	0.223	0.215
Flag21 on	-0.069	-0.023	0.005	0.276	0.225	0.217
Flag23 on	-0.052	-0.009	0.019	0.250	0.212	0.204
All on	-0.045	-0.005	0.023	0.232	0.203	0.195

566 Note: The function of each flag is to exclude level 2 pixels associated with:
 567 Flag5: wind speed retrieved from scatterometer HH-pol greater than 15 m/s
 568 Flag14: roughness correction not converging
 569 Flag17: difference between measured and predicted T_B exceeding 0.4 K
 570 Flag18: sea surface temperature below 5 °C
 571 Flag19: possible contamination from radio frequency interference
 572 Flag21: contamination from moon or galactic reflection
 573 Flag23: unacceptable ascending/descending difference

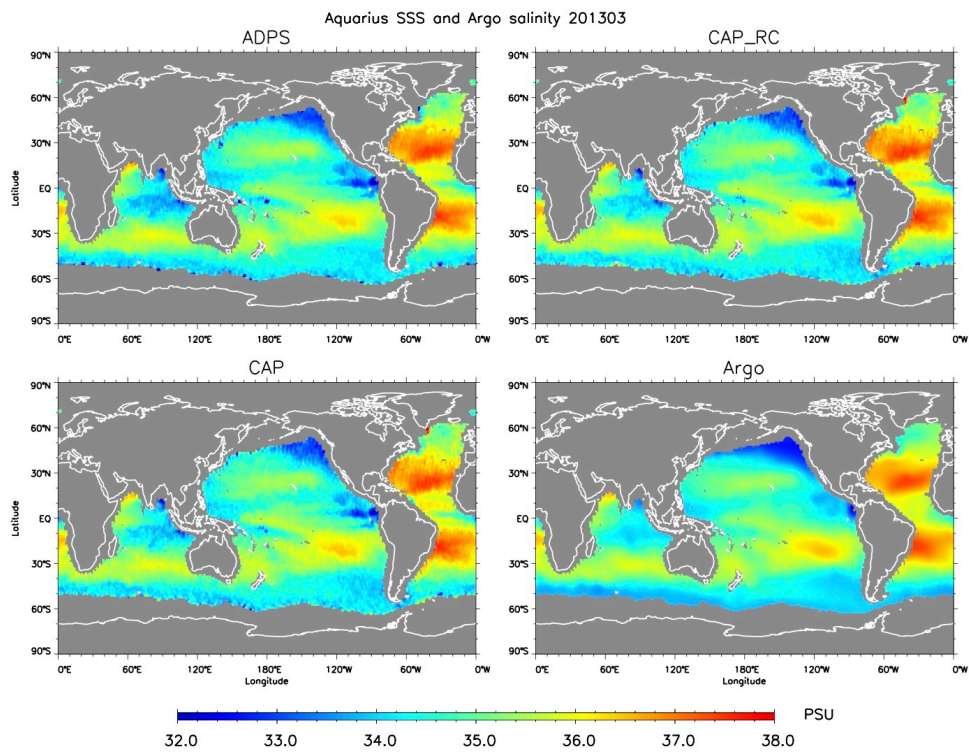
574
 575
 576 Table 3. RMSD, standard deviation and bias of Aquarius SSS (level 3) with respect to
 577 monthly gridded Argo data from September 2011 to December 2013 between 40°S
 578 to 40°N over all grid points or excluding two areas around Eastern Pacific Fresh
 579 Pool and Amazon River Outflow as indicated in Fig. 13.

(PSU)	40°S-40°N			40°S-40°N, excluding EPFP, ARO		
	ADPS	CAP	CAP RC	ADPS	CAP	CAP RC
RMSD	0.2833	0.2286	0.2216	0.2433	0.1932	0.1872
Std	0.2767	0.2283	0.2212	0.2383	0.1932	0.1859
Bias	-0.0607	-0.0119	0.0135	-0.0494	-0.0031	0.0221

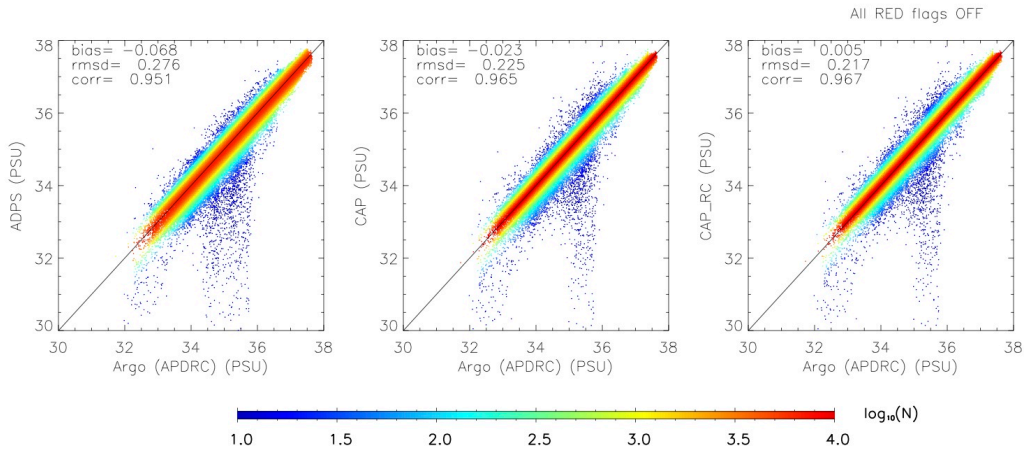
580



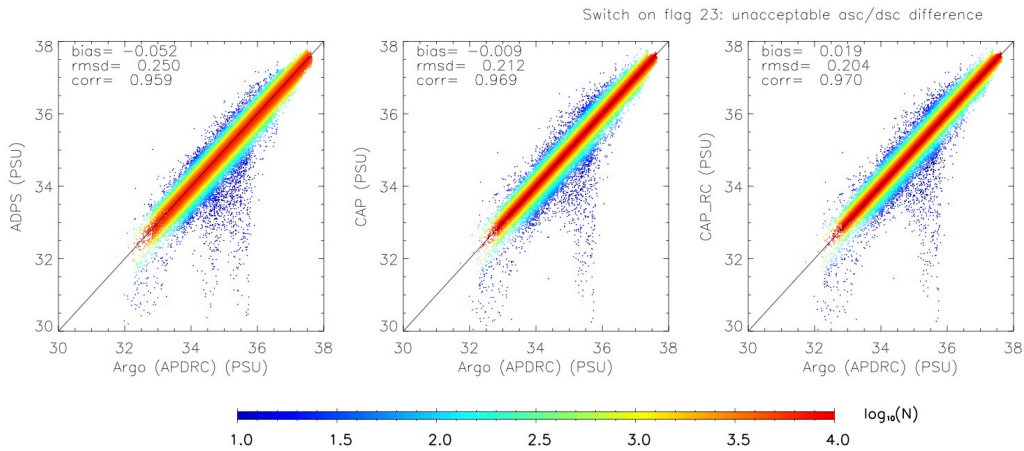
581
 582 Figure 1. Scatter plots of the Aquarius retrieved SSS ADPS (left), CAP (middle) and
 583 CAP_RC (right) vs. Argo floats matchups from August 25, 2011 to December 31,
 584 2012 for (top to bottom) all beams and beam-1, 2, 3 respectively.



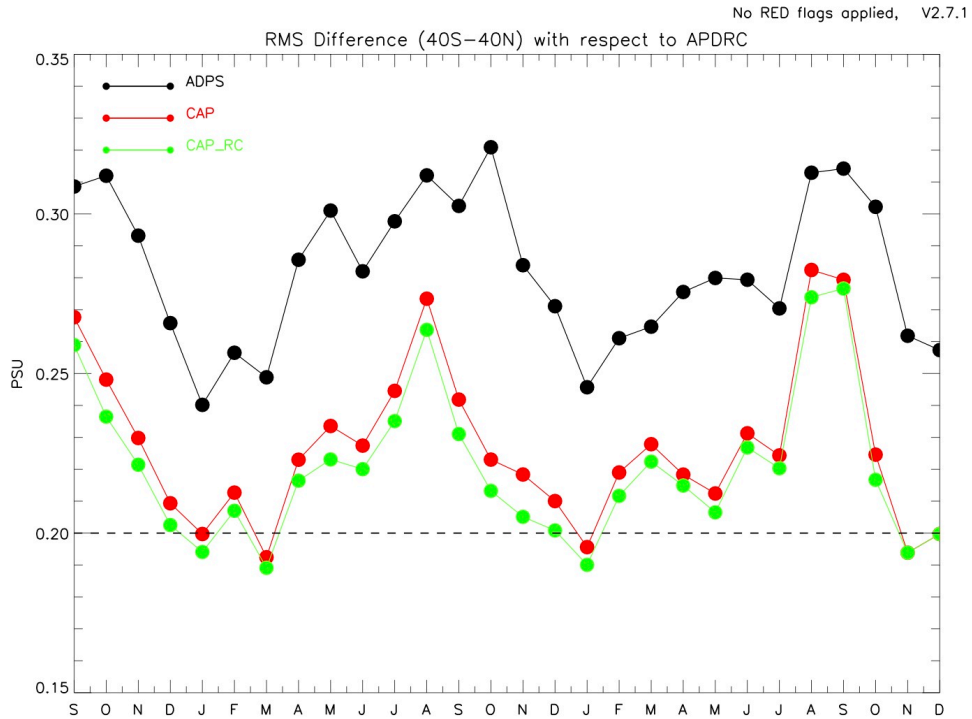
585
 586 Figure 2. The sea surface salinity maps of ADPS, CAP, CAP_RC, and APDRC Argo for
 587 the month of March 2013 on 1°x1° grid.



591
 592 Figure 4. Scatter plots of the Aquarius retrieved SSS (from left to right): ADPS,
 593 and CAP_RC vs. Argo, created from 12 monthly 1x1 gridded data between 40°S and
 594 40°N from 2012.

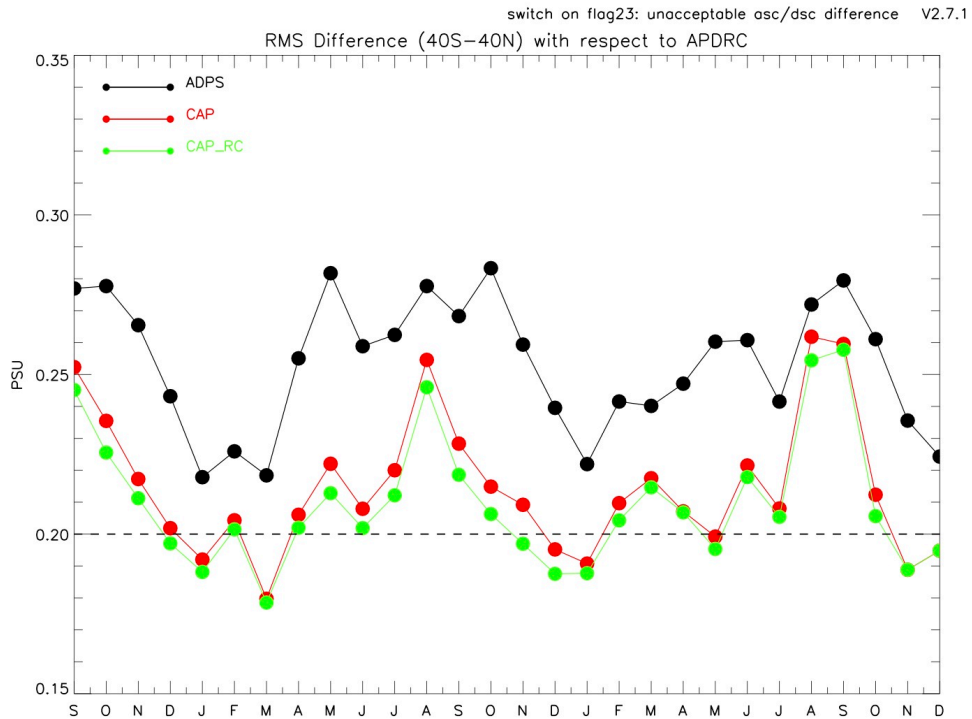


595
 596 Figure 5. Same as Fig. 4 with radiometer flag used to exclude additional data blocks
 597 with “unacceptable ascending/descending difference” in gridding.
 598



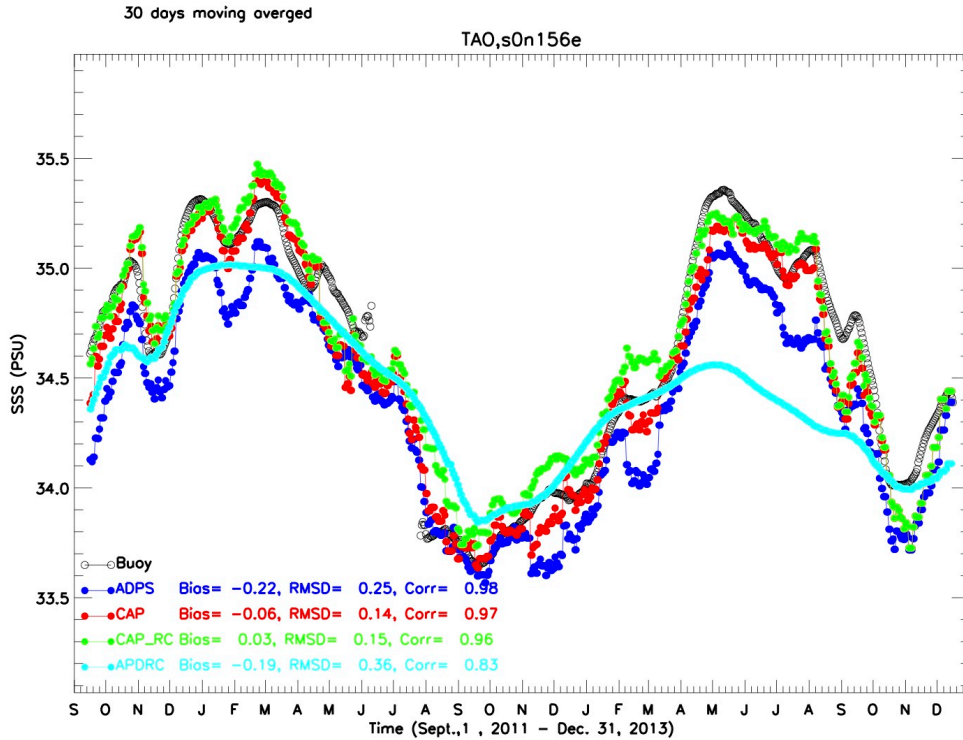
599
600
601
602
603

Figure 6. Time series of monthly RMS difference for Aquarius SSS ADPS (black), CAP (red) and CAP_RC (green) with respect to Argo data between 40°S and 40°N. Data blocks with land and ice fractions larger than 0.001 are not used in gridding.

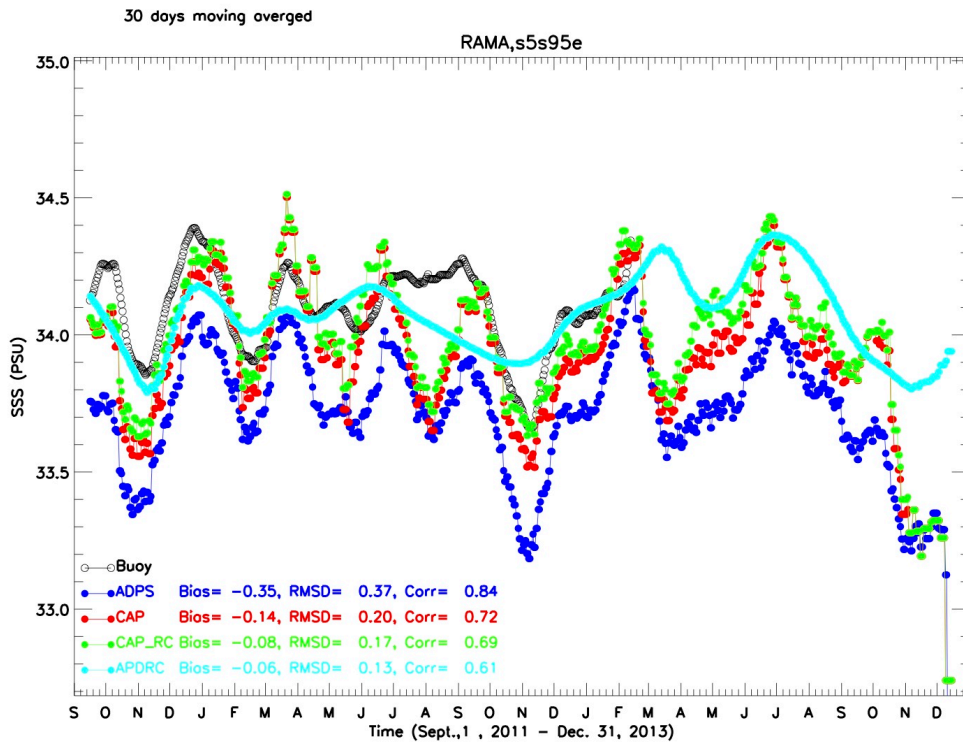


604
605
606

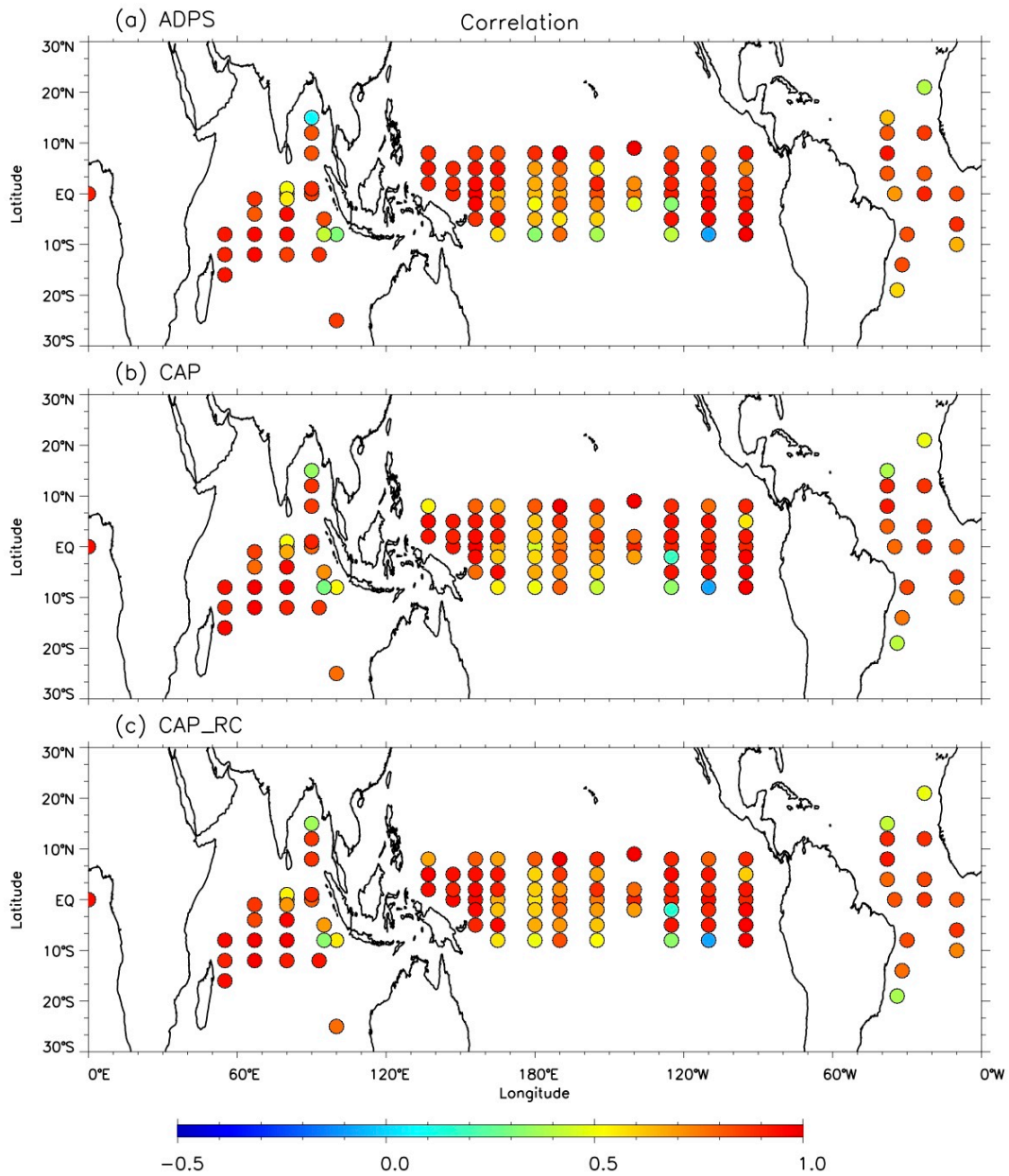
Figure 7. Same as Fig.6 with radiometer flag (bit 23) used to exclude additional data blocks with “unacceptable ascending/descending difference” in gridding.



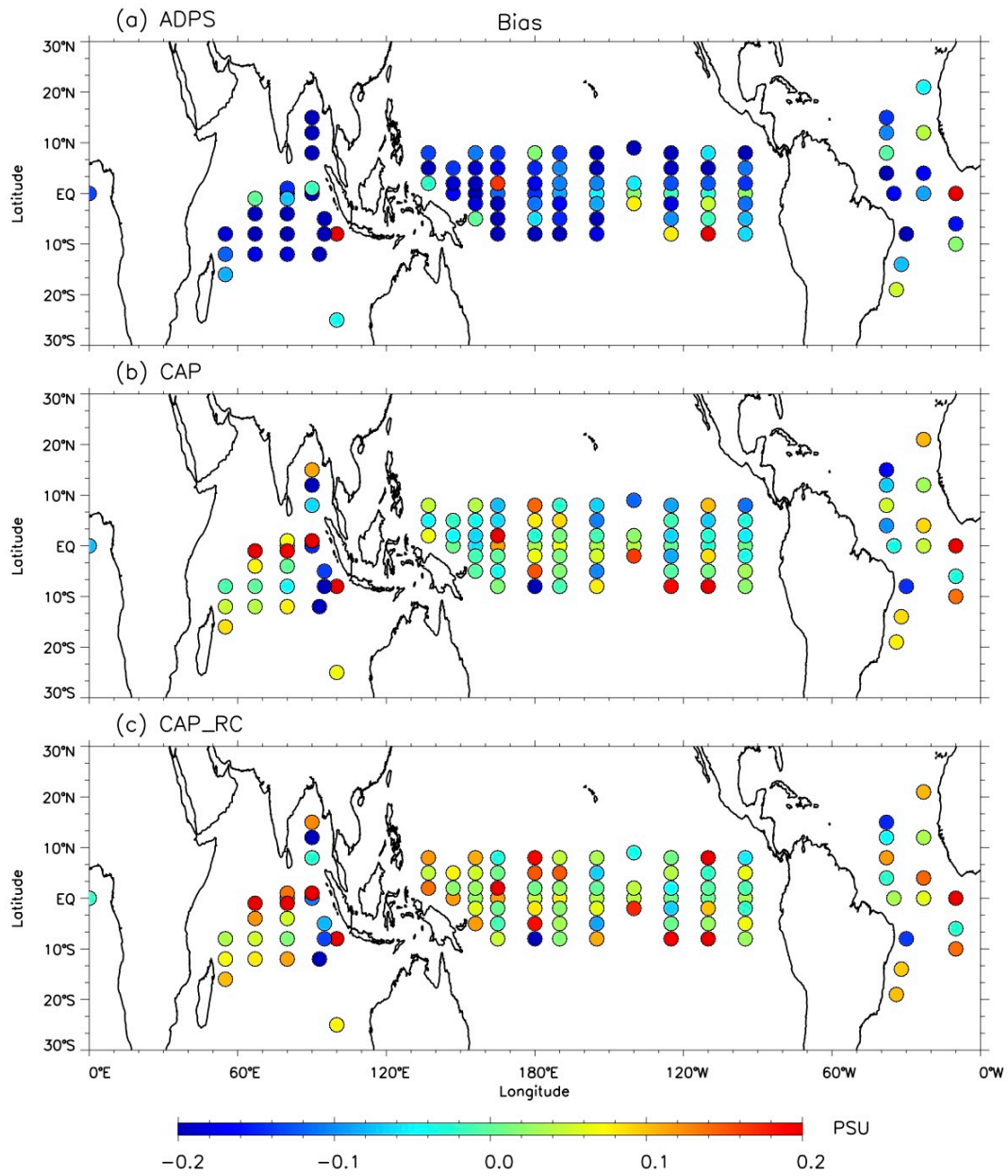
607
 608 Figure 8. (a) Time series of 30-days moving averaged buoy and Aquarius SSS at TAO
 609 buoy location 0°N, 156°E for buoy 1-m salinity (black): ADPS (red), CAP (blue),
 610 CAP_RC (green), and Argo (cyan).



611
 612 Figure 8. (b) Similar to Fig.8a, at RAMA buoy location 5°S, 95°E.

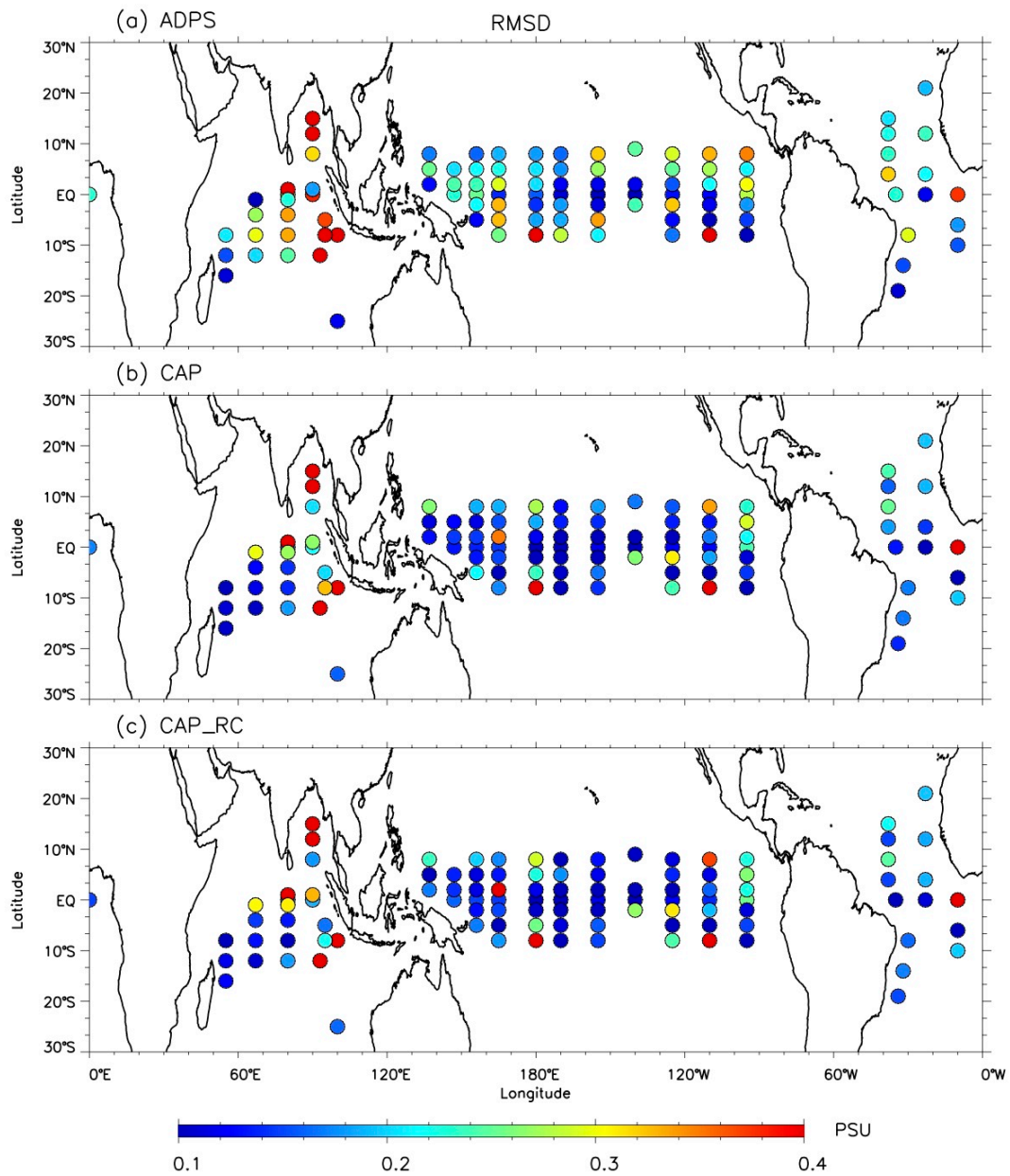


613
 614 Figure 9. At locations of the global tropical moored buoy arrays, the correlation
 615 coefficients between buoy 1-meter salinity and Aquarius derived SSS (a) ADPS, (b)
 616 CAP, and (c) CAP_RC, based on available daily records from Sept. 1, 2011 to Dec. 31,
 617 2013 (30 days moving average).



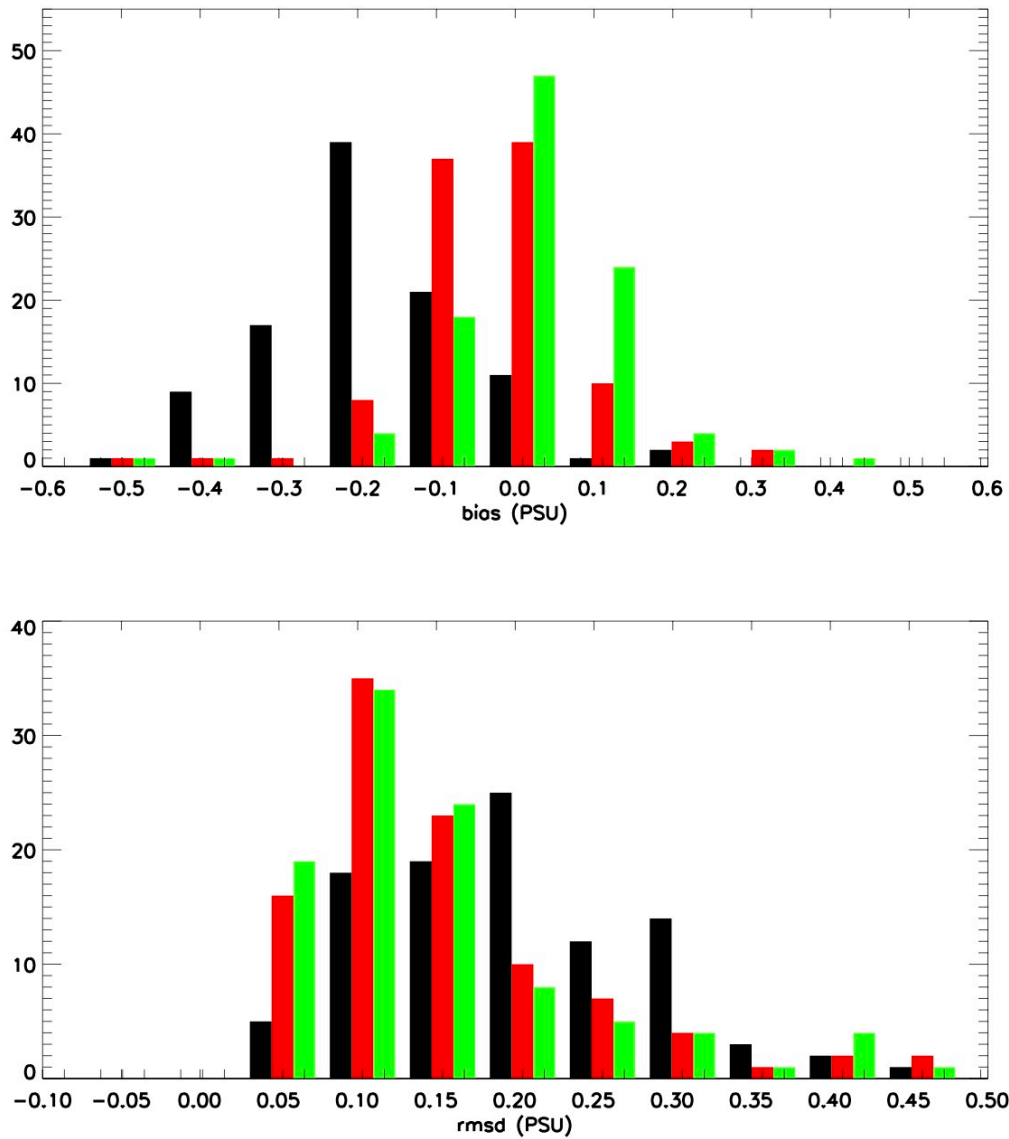
618
 619
 620
 621

Figure 10. Similar to Fig. 9, the bias of Aquarius SSS minus buoy 1-m salinity.

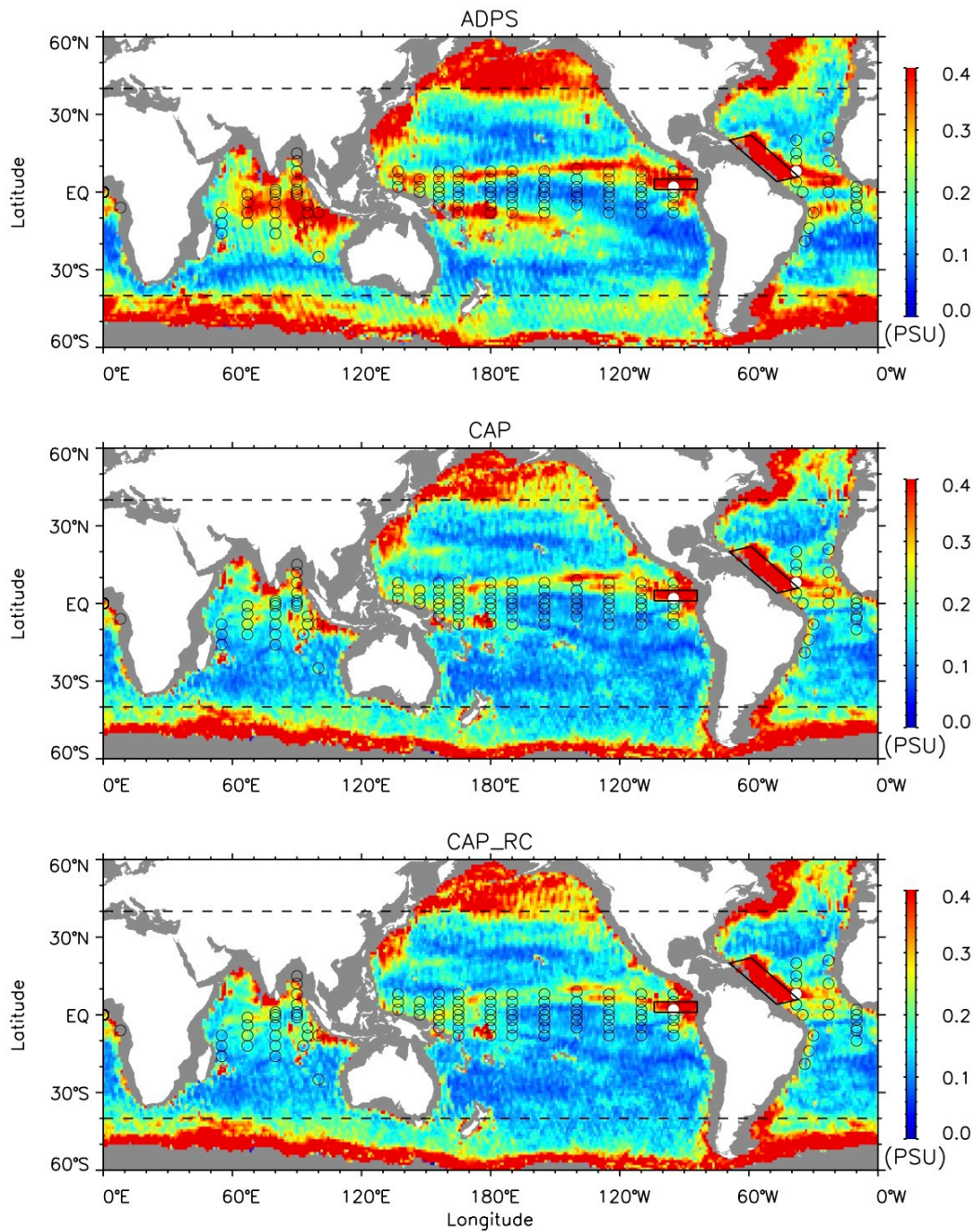


622
 623
 624
 625
 626
 627
 628
 629
 630

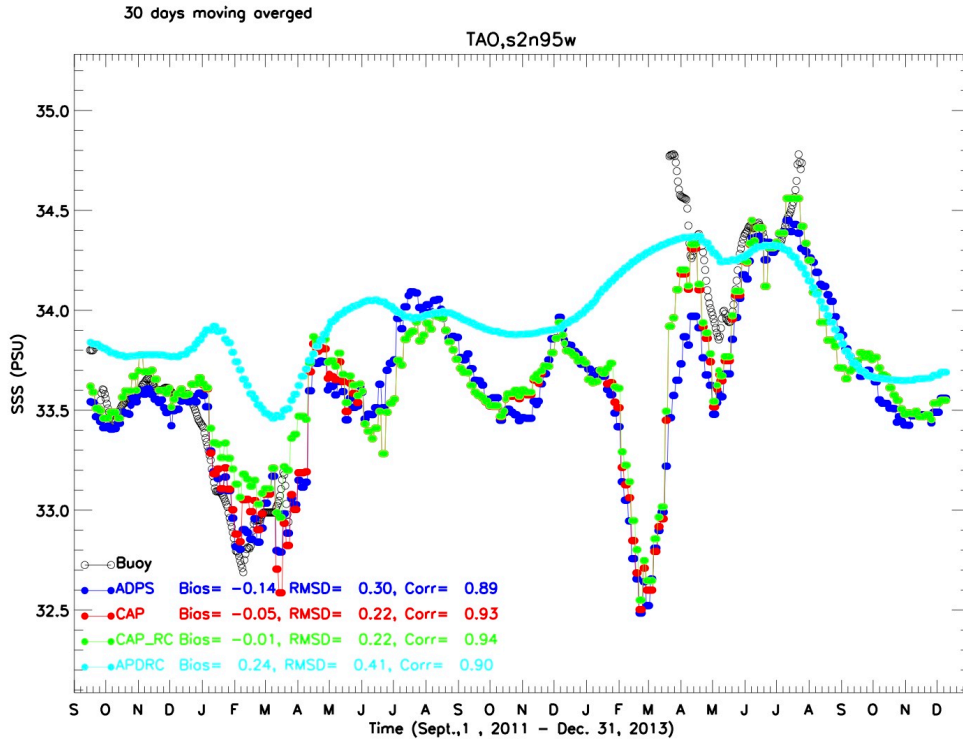
Figure 11. Similar to Fig. 9, the RMS difference between Aquarius SSS buoy 1-m salinity.



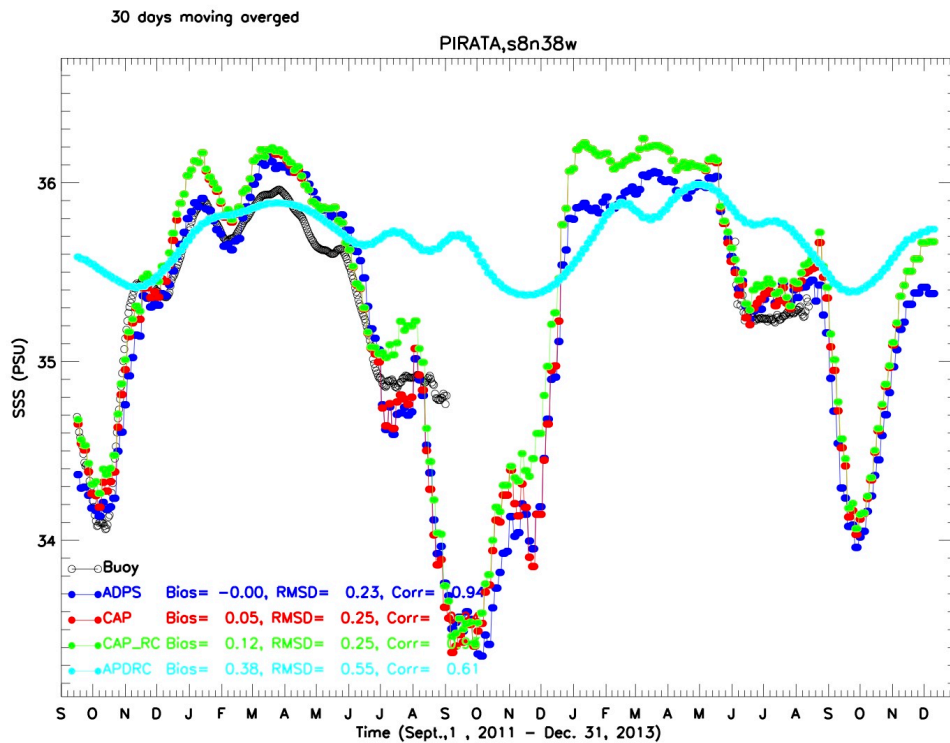
631
 632 Figure 12. Histogram of bias and RMS difference between Aquarius SSS: ADPS
 633 (black), CAP (red), CAP_RC (green), and buoy measured salinity at 1m over all
 634 locations of the global tropical moored buoy arrays, based on available 30-days
 635 moving averaged daily records from Sept. 1, 2011 to Dec. 31, 2013.
 636
 637



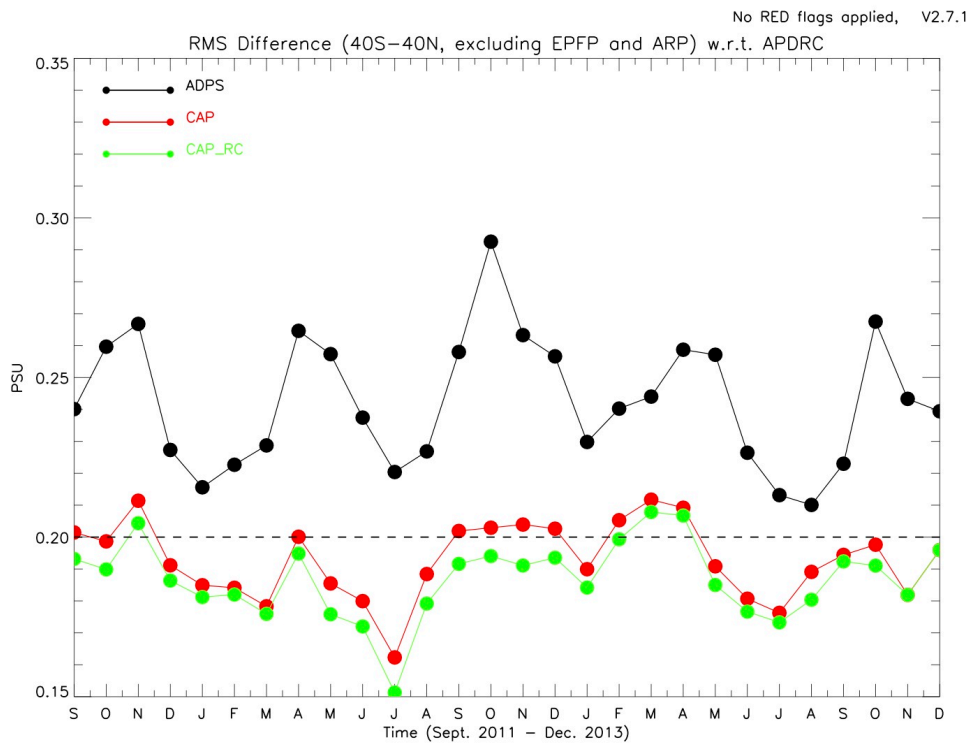
638
 639 Figure 13. RMS difference between Argo and Aquarius SSS ADPS (top),
 640 CAP (middle),
 641 CAP_RC (bottom) derived from 28 months of gridded data. Open circles are
 642 locations of the global tropical moored buoys. White dots indicate the locations of
 643 the time series shown in Fig. 14. The regions enclosed by solid lines are to be
 644 excluded in the monthly RMSD calculation shown in Fig. 15.



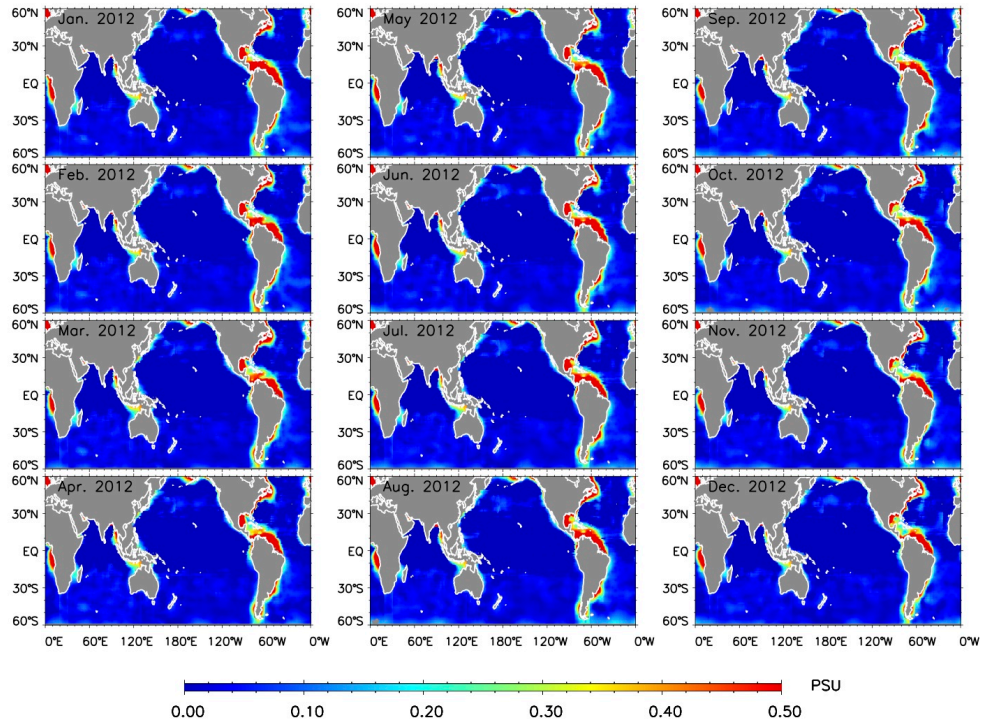
645
 646 Figure 14. (a) Daily time series of 30-days moving averaged buoy 1-m salinity (black
 647 circle) and Aquarius SSS ADPS (blue), CAP (red) and CAP_RC (green), and Argo
 648 (cyan) at TAO buoy location of 2°N, 95°W.
 649



650
 651 Figure 14. (b) Same as (a) at PIRATA buoy location of 8°N, 38°W.



652
 653 Figure 15. Similar to Fig. 6, the monthly time series of RMSD w.r.t. Argo between
 654 40°S and 40°N, excluding two regions in the Eastern Pacific Fresh Pool and the
 655 Amazon River plume (two patches enclosed by the solid lines in Fig. 13).
 656



657
658

Figure S1. Monthly maps of Argo OI error estimation for year 2012 from JAMSTEC.